

# Fast Nanoliter-Scale Cell Assays Using Droplet Microarray–Mass Spectrometry Imaging

Carina Ramallo Guevara, Dorothea Paulssen, Anna A. Popova, Carsten Hopf,\* and Pavel A. Levkin\*

In pharmaceutical research and development, cell-based assays are primarily used with readout that rely on fluorescence-based and other label-dependent techniques for analysis of different cellular processes. Superhydrophobic–hydrophilic droplet microarrays (DMA) and matrix-assisted laser desorption/ionization (MALDI) mass spectrometry (MS) have recently emerged as key technologies for miniaturized high-throughput cell assays and for label-free molecular high-content drug profiling, respectively. Here, nanoliter-scale cell assays are integrated on DMAs with MALDI–MS imaging (MALDI–MSI) approaches to a droplet microarray–mass spectrometry imaging (DMA–MSI) platform. Using A549 lung cancer cells, concentration-response profiling of a pharmaceutical compound, the fatty acid synthase inhibitor GSK2194069, are demonstrated. Direct cell culture on DMAs enables combination of microscopy and high speed, high molecular content analysis using MALDI–MSI. Miniaturization of array spots down to 0.5 mm confining 40 nL droplets allows for MALDI imaging analysis of as few as ten cells per spot. Partial automation ensures a fast sample preparation workflow. Taken together, the integrated DMA–MSI platform that combines MALDI–MSI, as a label-free analytical readout, with the miniaturized droplet microarray platform is a valuable complement to high throughput cell-based assays technologies.

## 1. Introduction


High-throughput drug screening in live cells is widely used in fundamental research and drug discovery.<sup>[1]</sup> More than half of the small-molecule drugs approved in the last decade were discovered using phenotypic cell-based assays.<sup>[2]</sup> Herein, cells are used as simplified disease models that are incubated with compounds in vitro to search for desirable cellular phenotypes. Any drug-like compound can interfere with multiple cellular processes, including cell signaling, metabolism, protein expression, secretion, progression of the cell cycle or cell death.<sup>[3]</sup> Complementing phenotypic assays, mechanistic cell-based assays measure pharmacodynamic (PD) markers in cells, either alone or in small combinations, which indicate how a compound penetrates the cell and how it engages a defined pharmacological target. The most common methods for detecting such changes include microscopy, bulk solution assays, or off-line bioanalytical assays.<sup>[4]</sup> These methods usually require specific labels to quantify the change in cell phenotype, or multistep biochemical work-

ups to quantify the PD biomarker. With microscopy-based readouts, specific antibodies or special dyes are commonly used to visualize different cell processes; for example, propidium iodide staining is used to assess apoptosis, calcein staining is used to estimate cell viability, and anti-Ki67 antibody labeling is used to assess cell proliferation.<sup>[5]</sup> PD drug responses can be monitored by changes in biomolecular cell composition. Label-free readout methods can enable an unprecedented view of how drug treatment affects the composition and modification of cellular biomolecules beyond expected target molecules.

Many label-free analytic technologies lack the molecular specificity (e.g., spectroscopic methods), the speed required for high-throughput cell assays, or they are not able to be used in matrices as complex as cells (e.g., nuclear magnetic resonance or surface plasmon resonance). Chemical sensors and artificial receptors, such as cyclodextrins or cucurbiturils, can only be applied to specific analytes. Moreover, apart from spectroscopic methods, none of these techniques allow spatial probing of a single cell culture—something that is important due to heterogeneous cell responses and cell-to-cell variation and, which is necessary to predict the pharmacological ability of compounds to tackle unmet medical needs.<sup>[6]</sup>

Dr. C. Ramallo Guevara, Prof. C. Hopf  
Center for Mass Spectrometry and Optical Spectroscopy (CeMOS)  
Mannheim University of Applied Sciences  
Paul-Wittsack Str. 10, Mannheim 68163, Germany  
E-mail: c.hopf@hs-mannheim.de

D. Paulssen, Dr. A. A. Popova, Prof. P. A. Levkin  
Karlsruhe Institute of Technology (KIT)  
Institute of Biological and Chemical Systems – Functional Molecular  
Systems (IBCS-FMS)  
Hermann-von-Helmholtz-Platz 1, Eggenstein-Leopoldshafen 76344,  
Germany  
E-mail: levkin@kit.edu

 The ORCID identification number(s) for the author(s) of this article can be found under <https://doi.org/10.1002/adbi.202000279>.

© 2021 The Authors. Advanced Biology published by Wiley-VCH GmbH. This is an open access article under the terms of the Creative Commons Attribution-NonCommercial License, which permits use, distribution and reproduction in any medium, provided the original work is properly cited and is not used for commercial purposes.

DOI: 10.1002/adbi.202000279

Matrix-assisted laser desorption/ionization (MALDI) mass spectrometry (MS) is fast, compatible with high-throughput screening, reasonably quantitative, covers a variety of biomolecular classes and, through MS imaging (MSI), supports spatially resolved analysis down to a single cell within a population. In recent years, MALDI-MS has emerged as a leading analytical tool in cell-based drug discovery and profiling.<sup>[7–12]</sup> It is a versatile technology for the label-free analysis of various classes of molecules, and is fast becoming established as a high-throughput method for biochemical screening assays.<sup>[12–14]</sup> In non-pharmacological applications, the utility of MALDI-MS for single cell metabolite analysis has been demonstrated, including in microcavity arrays.<sup>[15–17]</sup> Compared with commonly used fluorescence- and chemiluminescence-based readouts, which require costly and non-physiological secondary probes and therefore suffer from false-positive and false-negative results,<sup>[14]</sup> MALDI-MS is label-free and allows multiple components to be detected simultaneously.<sup>[12]</sup>

Recently, MALDI-MS has also been adopted to analyze changes in the biomolecular composition of whole cells—both microbial,<sup>[18]</sup> and mammalian<sup>[7,9,12,19]</sup>—after treatment with putative therapeutic compounds. Since hundreds of molecules can be detected simultaneously, MALDI-MS can identify PD effects in cells at the lipid or metabolic level using computational workflows.<sup>[10]</sup> Concentration-dependent molecular changes can be measured for known and directly affected abundant proteins (e.g., polyacetylated histones), or for low molecular mass PD markers in mammalian cells.<sup>[7,9,19]</sup> For example, to profile cellular levels of potential fatty acid synthase (FASN) in K562 cells, MALDI-MS has been used to determine the accumulation of malonyl-coenzyme A (CoA), the substrate of FASN.<sup>[9]</sup>

MALDI-MS can detect multiple analytes in parallel and in a high throughput manner. This makes it an attractive candidate for adaptation to a label-free detection method in high-throughput screening applications. However, one drawback is that the multi-well plates commonly used for biochemical and cell-based assays, which provide separated reservoirs for multiple single biological experiments in parallel, cannot be used for MALDI-MS directly. This is because they are incompatible with lasers, and are made from non-conductive polystyrene; for high ion yield and strong signal readout, an appropriate conductive substrate must be chosen.<sup>[20]</sup> Therefore, if MALDI-MS is to be used in a high throughput context, analytes or cells must be transferred from multi-well plates onto special MALDI plates, or onto microarrays for mass spectrometry.<sup>[7,9,12–15,17,19]</sup> This step can be automated for measuring analytes in solution, but cannot be done to detect the biomolecules of intact treated cells directly on the platform.<sup>[14]</sup>

Recently, we developed a miniaturized cell screening platform based on arrays of sub-100 nL droplets. These are formed in 0.5–3.0 mm hydrophilic spots, separated by superhydrophobic regions.<sup>[21,22]</sup> Such “droplet microarrays” allow drug screening to be conducted in up to 1000-fold lower volumes, with proportionally lower quantities of reagents and cells. This not only reduces the cost of drug screening, but also helps to enable disease-relevant screening of rare and primary cells, such as stem cells and patient-derived cells. This ground breaking experimental approach has great potential for diverse applications, including

combination of chemical synthesis and biological screening, as well as various readout formats and analytics approaches.

Until now, droplet microarray cell screening has been performed using established fluorescence microscopy readouts. In this study, we present a novel MALDI-on-a-chip platform called Droplet Microarray–Mass Spectrometry Imaging (DMA–MSI). The DMA–MSI platform enables cell-based compound profiling or screening in droplets in nanoliter- or microliter scale volumes. This is, followed by microscopy and consequent measurement of PD markers by MALDI–MSI directly on the array, without the need to transfer cells to a specialized MALDI plate. We demonstrate the feasibility of our new platform for monitoring the intracellular accumulation of malonyl-CoA in A549 cells, in response to the selective, small FASN inhibitor GSK2194069. This approach enables highly miniaturized, cell-based, high-throughput assays combined with both optical and sensitive label-free MSI readouts on a chip. The DMA–MSI platform reveals new opportunities to monitor pharmacodynamics in live cells, which is crucial for drug discovery and precision medicine.

## 2. Results and Discussion

We have developed the versatile DMA–MSI platform, which combines a droplet microarray (DMA) platform for the high-throughput screening of live cells, with MALDI–MS imaging for label-free pharmaceutical bioanalysis of cells on a single array. In **Figure 1**, the rapid work-flow from customized array manufacturing, cell culture on array, sample preparation, measurement and data analysis are shown. Droplet microarrays are planar, wall-less arrays of hydrophilic spots in a superhydrophobic background, which enable dense arrays of stable, separated droplets to be formed in the order of nanoliter to microliter volumes. Advantages of the DMA platform for cell screening include its high-throughput ability (80–4500 spots per microscope glass slide), miniaturized format (up to 10<sup>3</sup>-fold reduction in reagent and cell volume), versatility (compatibility with all types of cells and 2D and 3D cell culture models), and compatibility with existing high-content screening workflows based on microscopy-based readouts.<sup>[22,23]</sup> Its planarity and ability to confine low volumes in defined areas also offer unique features crucial for MALDI-MS imaging. Therefore, DMA combines advantages for screening live cells and MALDI-MS analysis, making it possible to perform both on the same platform.

### 2.1. Preparation of DMA-ITO Slides

As a first step, we have established DMAs on a conductive surface, which is necessary for MALDI–MSI. DMAs were prepared on transparent indium tin oxide (ITO)-coated slides. The coating renders the surface conductive, with a resistance of 150–170 Ω sq<sup>-1</sup>; this is important to be able to achieve high-sensitivity MALDI–MSI measurements in high-vacuum ion sources. To evaluate the ability to miniaturize the DMA–ITO slides, we prepared DMA–ITO slides with spots of different sizes: 3, 1, and 0.5 mm. The receding water contact angle was close to 0 and hard to measure owing to high hydrophilicity.

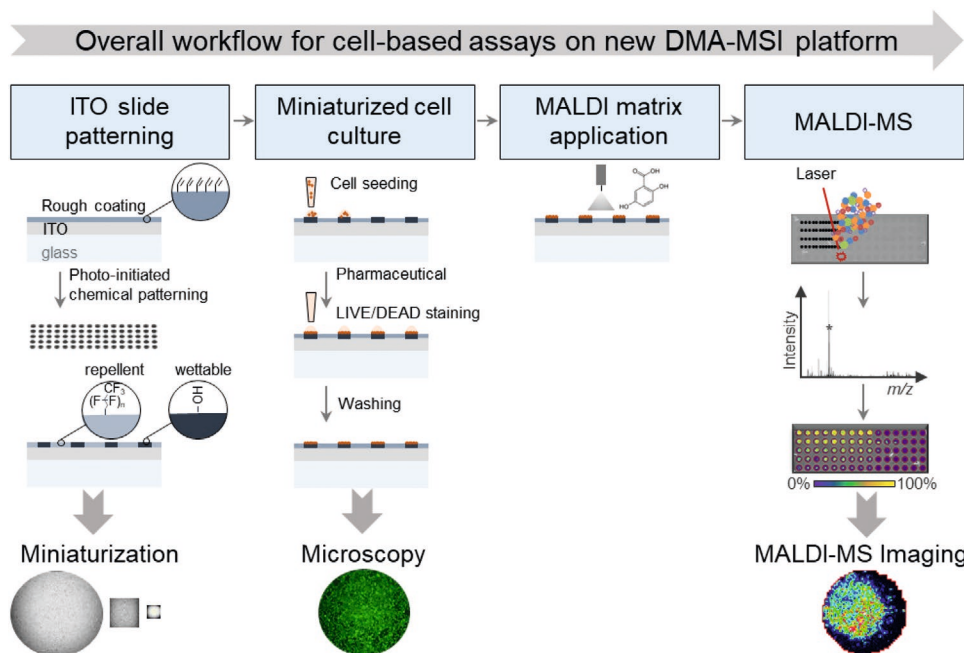


**Figure 1.** Integration of DMA–ITO Slides and MALDI–TOF–MSI to a Technology Platform for Label-free Cell-based Assays. Combining miniaturized high-throughput cell screening based on droplet microarrays (DMA) on conductive indium tin oxide (ITO) glass slides, with high-content bioanalysis using matrix-assisted laser desorption/ionization–time-of-flight–mass spectrometry imaging (MALDI–TOF–MSI) enables cell-based assays for cell and drug screening. The platform enables direct cell culture on DMA–ITO slides, cell treatment and the possibility to perform microscopy applications as well as MALDI–TOF–MSI analyses. The workflow includes: a) ITO slide patterning to create an array of hydrophilic spots on a superhydrophobic surfaces; b) seeding and culturing cells in nanoliter droplets on the chip, followed by microscopy readout; c) application of MALDI matrix, and d) MALDI-MS imaging of cells in each hydrophilic spot, followed by data analysis.

The background of the array was shown to be superhydrophobic with static water contact angle and sliding angles being  $160^\circ$  and  $5.3 \pm 2.2$ , respectively. Such a large difference in hydrophilicity is important to confine cell suspensions or MALDI matrix solutions with different volumes to hydrophilic spots.

## 2.2. MALDI–MSI Optimization

To test the effect of surface patterning on MALDI–MS analysis, we first added 5  $\mu\text{L}$  of cell culture medium to 3 mm hydrophilic spots. Unlike non-patterned ITO, the DMA–ITO slides ensured uniform, compact and constant droplets of cell culture medium; this is a prerequisite for successful cell culture, especially in miniaturized nanoliter (spot size < 1 mm) formats (Figure 2A). Indeed, the ability to create liquid droplets with footprints of defined geometry and size was shown to be important for the crystallization of 2,5-dihydroxybenzoic acid (DHB) matrix, whether alone or in dried droplet mixtures with a brain lipid extract. In this study, homogeneously distributed matrix-analyte co-crystals were formed on DMA–ITO rather than matrix crystallization from droplets on non-patterned ITO slides (Figure 2B). This improved matrix crystallization was found to be important to enhance homogeneity of the MS signals; for example, the exemplary peak at  $m/z$  760.6, which presumably corresponds to the protonated abundant membrane phospholipid phosphatidylcholine (PC, 34:1) across the spots (Figure 2C). Several studies have noted the importance of uniform, homogeneous spots in MALDI–MS assays.<sup>[10,11,24]</sup> It is

well known that DHB matrix can form inhomogeneous spots, with greatly varying intensities of analyte ions across the spot. This has prompted some authors to stop using it in assays, and others to employ matrix sprayers to prepare samples by spray-coating rather than dried droplets.<sup>[10,11]</sup>

We also compared the intensity of MS signals, and sensitivity of the measurements to evaluate total brain lipid extracts co-crystallized with DHB matrix on functionalized versus non-functionalized ITO slides (Figure S1, Supporting Information). The results demonstrated no reduction in MS sensitivity, which might otherwise occur because of the potential for the additional coating to create superhydrophobic–hydrophilic patterns insulating the underlying conductive substrate. Therefore, we demonstrated that better confinement of analytes and improved homogeneity of matrix crystallization on DMA–ITO slides are possible, compared with standard ITO slides, with no loss of sensitivity in MS measurements.

## 2.3. Cell Culture on DMA–ITO Slides

To test the biocompatibility of the patterned ITO slides, we cultured A549 lung cancer cells in 5  $\mu\text{L}$ , 150 nL, and 40 nL droplets, confined in 3, 1, and 0.5 mm hydrophilic spots, respectively. Using a non-contact liquid dispenser, the cells were dispensed directly onto the hydrophilic spots, which allowed droplet volume control down to a few nanoliters, as well as control of the number of cells per spot by adjusting printing volumes and cell concentration. Initially, we used a constant cell density of

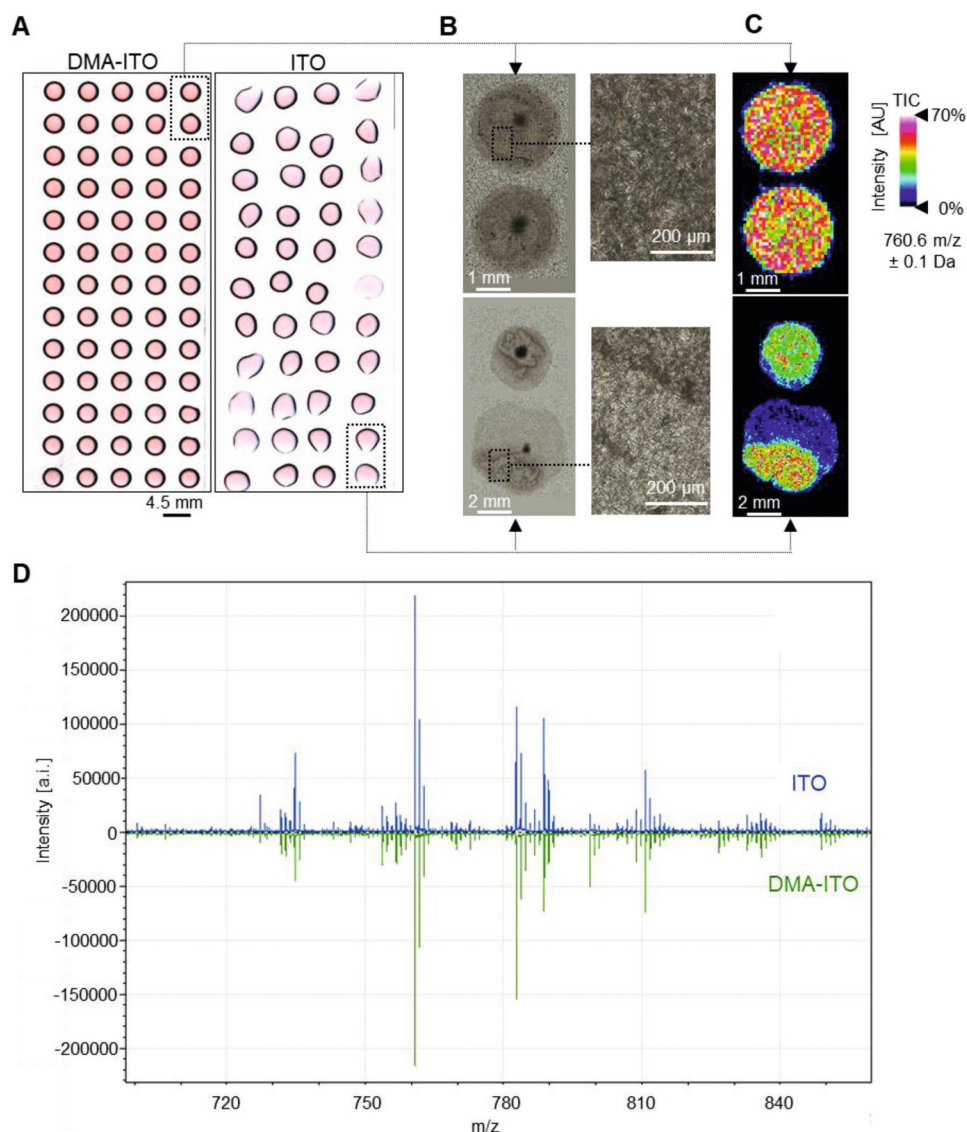


**Figure 2.** Features of Microstructured ITO Slides Compared with Conventional Usage of ITO Slides for Spatially Resolved MALDI-MS Imaging. A) Droplet microarray-indium tin oxide (DMA-ITO) slides ensure that cell culture media form uniform, compact, constant droplets. B) Efficient matrix/analyte co-crystallization caused by compact and stationary droplet formation on DMA-ITO, which leads to consistent distribution of ion intensities. C) Exemplary total ion count (TIC)-normalized matrix-assisted laser desorption/ionization-mass spectrometry (MALDI-MS) ion image showing the spatially resolved lipid distribution of  $m/z$  760.6, presumably corresponding to the protonated phosphatidylcholine (PC, 34:1). D) Signal intensities of TIC-normalized mean spectra extracted from regions of interest (ROI) from ITO (blue) versus DMA-ITO (green) are comparable. No additional  $m/z$  peaks were detected owing to the nanorough coating. Data processing was carried out using SCiLS Lab, and TIC-normalized mean spectra of ROI drawn in SCiLS Lab were exported into mMass, in order to flip spectra vertically to detect possible differences.

141 cells  $\text{mm}^{-2}$ , (corresponding to 1000, 111 and 28 cells per array spot on 3, 1, and 0.5 mm DMA, respectively). Cells were cultured on the DMA-ITO slides for 18 h in a humidity chamber, which was placed in a regular cell culture incubator. To evaluate their viability, cells were stained with calcein (indicating viable cells) and propidium iodide (PI, an indicator of dead cells) by printing corresponding reagents directly into the spots. As judged by fluorescence microscopy imaging, the viability of all tested culture volumes and cell densities was above 90%. This demonstrates good biocompatibility of the novel DMA-ITO slides, and the possibility to greatly miniaturize cell experiments using 0.5 mm spots and 40 nL droplets (Figure 3A). Cell

viability remained above 90% at higher (707 cells  $\text{mm}^{-2}$ , corresponding to 5000, 555, and 138 cells per array spot on 3, 1, and 0.5 mm DMAs, respectively) and lower cell densities (14 cells  $\text{mm}^{-2}$ , corresponding to 100, 11, and 3 cells per array spot on 3, 1, and 0.5 mm DMAs, respectively) (Figure 3D).

#### 2.4. MALDI-MSI of Whole Cells Cultured Using DMA-ITO Slides

Next, we investigated the possibility of combining miniaturized cell experiments using 5 μL to 40 nL droplets formed on a

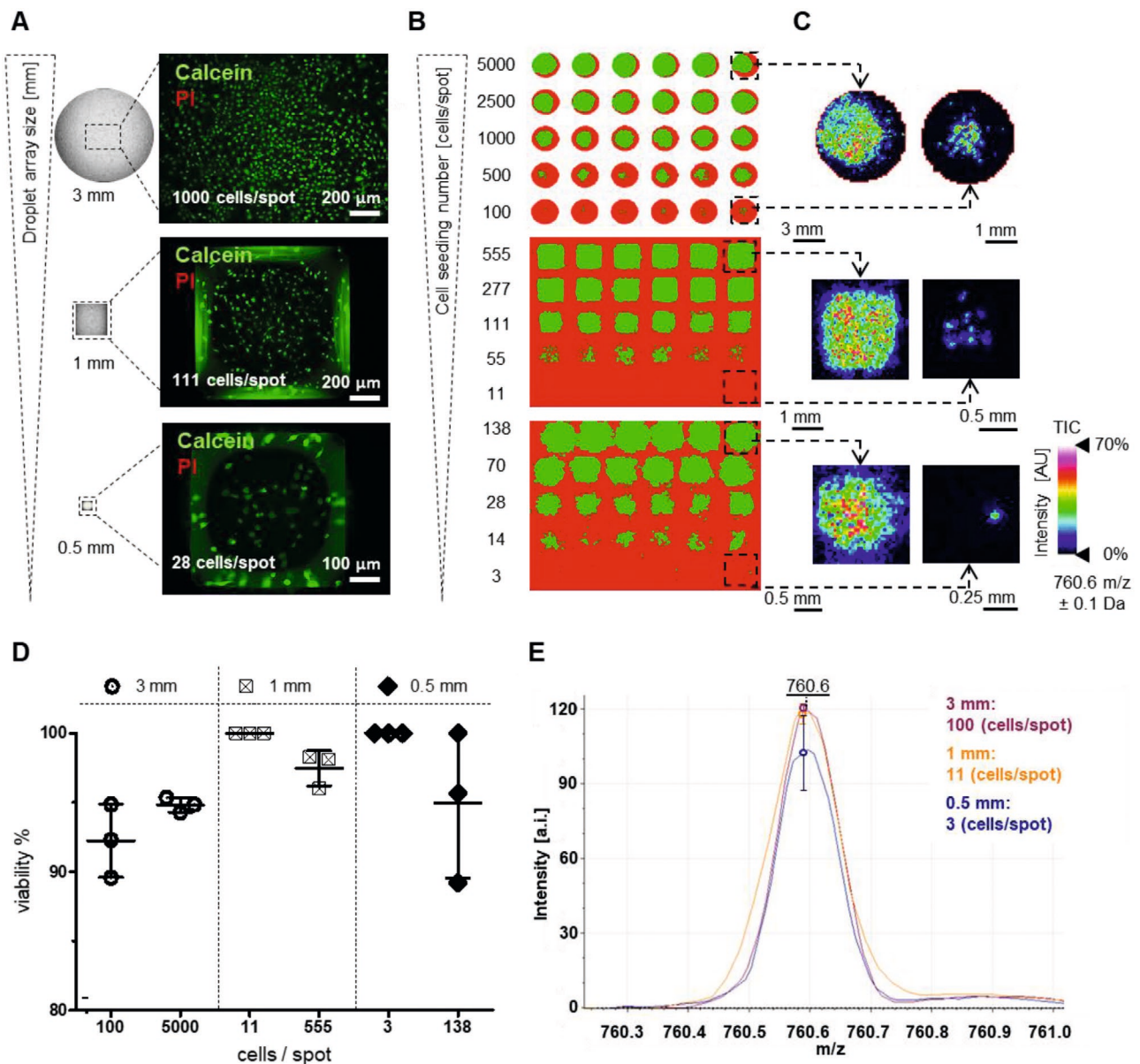


**Figure 3.** Miniaturized A549 Cancer Cell Culture on Different DMA-ITO Formats. A) Proportional down-scaling of cell number per array spot on 3, 1, and 0.5 mm droplet microarray-indium tin oxide (DMA-ITO). Shown are droplet array size, shape, and corresponding cell numbers per spot. Demonstration of biocompatibility for cells cultured on DMA-ITO. Cell viability testing (calcein staining; green) after cultivation overnight showed >90% viable cells and lack of toxicity (dead cell indicator propidium iodide (PI); red) resulting from photochemical microstructuring on ITO glass. B) To analyze miniaturized cell cultures, A549 cells were seeded at different cell numbers per spot, representing constant cell densities (cells/mm<sup>2</sup>) to study the various DMA-ITO spot sizes (3, 1, 0.5 mm). Spatial segmentation by bisecting *k*-means clustering with *k* = 2 of matrix-assisted laser desorption/ionization-mass spectrometry imaging (MALDI-MSI) datasets acquired on differently sized DMA-ITO arrays distinguishes cell-bearing pixels (green) from matrix background (red) down to nearly the single-cell level. Data processing and unsupervised segmentation analysis was carried out using SCiLS Lab and results are shown for (*n* = 6) six technical replicates for each array size. C) Corresponding MALDI-MSI ion images show the spatial signal distribution of *m/z* 760.6, tentatively assigned to the protonated cell membrane lipid phosphatidylcholine (PC, 34:1) for the highest and lowest cell density seeded out on different array sizes. MSI data were acquired using a raster width of 50  $\mu$ m for the 3 mm slides, and 25  $\mu$ m for the 1 and 0.5 mm DMA-ITO slides, respectively. D) Shows over 90% cell viability monitored prior to MALDI-MSI measurements shown in (B) after overnight cell culture on DMA-ITO. Data were presented as mean  $\pm$  standard deviation (*n* = 3 technical replicates out of datasets from (B)). E) Original total ion count (TIC)-normalized spectra of *m/z* 760.6 from a signal-bearing pixel extracted from the respective array positions, with the lowest cell number per spot for the different array sizes were analyzed using the mMass open source mass spectrometry tool. Shown are means  $\pm$  standard deviation (SD) of three (*n* = 3) technical replicates from the dataset in (B).

**Table 1.** Seeding densities and volumes used for different array formats to keep the cell density per area ( $\text{mm}^2$ ) constant. Seeding volumes were 5  $\mu\text{L}$ , 150 nL, and 40 nL for 3 mm circular, 1 mm squared, and 0.5 mm squared array spots, respectively.

[Cells $\text{mm}^{-2}$ ]	Array size: $\varnothing$ 3 mm		Array size: 1 mm		Array size: 0.5 mm	
	No. cells/spot	Seeding density [cells $\text{mL}^{-1}$ ]	No. cells/spot	Seeding density [cells $\text{mL}^{-1}$ ]	No. cells/spot	Seeding density [cells $\text{mL}^{-1}$ ]
707	5000	$1 \times 10^6$	555	$3.7 \times 10^6$	138	$3.5 \times 10^6$
354	2500	$5 \times 10^5$	277	$1.8 \times 10^6$	70	$1.7 \times 10^6$
141	1000	$2 \times 10^5$	111	$7.5 \times 10^5$	28	$6.9 \times 10^5$
71	500	$1 \times 10^5$	55	$3.7 \times 10^5$	14	$3.5 \times 10^5$
14	100	$2 \times 10^4$	11	$7.5 \times 10^4$	3	$6.9 \times 10^4$

DMA-ITO slide with chemical analysis using MALDI-MSI on the same slide. A549 cells were cultured on DMA-ITO slides with different hydrophilic-superhydrophobic patterns to form arrays of 5  $\mu\text{L}$ , 150 nL and 40 nL droplets. The initial cell density varied from 14 cells/ $\text{mm}^2$  to 707 cells/ $\text{mm}^2$  (corresponding to seeded cell numbers indicated in **Table 1** and Figure 3B) to investigate different cell culture conditions. The viability of cells on DMA-ITO slides was confirmed by live/dead staining using fluorescence microscopy. Then, the same DMA slide was washed with ice-cold ammonium formate and air-dried slides were spray-coated with 60 mg/mL DHB matrix in in ACN/ddH<sub>2</sub>O/TFA (50/49.9/0.1;  $v/v/v$ ), followed by MALDI-MSI analysis in a RapifleX MALDI-TOF mass spectrometer. MSI data were acquired using a raster width of 50  $\mu\text{m}$  for the 3 mm DMA slides, and 25  $\mu\text{m}$  for the 1 mm and 0.5 mm DMA slides. Computational analysis of MALDI-MSI data was performed using SCiLS Lab software, using the spatial segmentation map generated by bisecting  $k$ -means clustering. Employing  $k = 2$  for the clustering, cell-bearing and non-cell-bearing pixels could conveniently be distinguished down to <10 cells per array spot (Figure 3B). Corresponding MALDI-MSI ion images show the spatial signal distribution of the abundant cell membrane lipid (presumably PC 34:1;  $m/z$  760.6; normalized to total ion current) for the highest and lowest cell density seeded out on different array sizes (Figure 3C). This indicates that cell membrane lipids can be detected and visualized on DMA-ITO slides down to single cell numbers. The spatial distribution of analytes of interest was visualized as ion intensity maps using SCiLS Lab software, which revealed the possibility of single cell imaging. The cell patterns formed by cells cultured inside droplets is clearly visible. Ion intensity of  $m/z$  760.6 was similar for various given cell densities, independent of the DMA format (3, 1, or 0.5 mm; Figure S2, Supporting Information). These results demonstrate that MALDI-MSI readout has potential sensitivity down to the single cell level. Combined with parallel optical microscopy readouts, high-throughput screenings and extreme miniaturization, this shows the unique potential for MALDI-MS imaging on the same platform as droplet microarray technology.

## 2.5. Quantitative Assessment of Biomarkers Using DMA-MSI Platform

GSK2194069 was chosen to demonstrate the possibility of using the DMA-MSI platform to functionally and quantitatively investigate PD biomarker changes in response to small molecule

drug-like compounds. GSK194069 is a selective fatty acid synthase (FASN) inhibitor, which leads to intracellular accumulation of the FASN substrate (and acetyl-CoA-carboxylase product) malonyl-CoA (**Figure 4A**), as demonstrated and analytically validated in a MALDI cell assay using steel targets.<sup>[9]</sup> To this end, A549 cells were cultured in 3 mm spots on an DMA-ITO slide for 18 h, then treated for 24 h in the presence of GSK2194069. This was followed by a spray-coat with MALDI matrix and analysis by MALDI-MSI directly on the slide. MALDI-TOF mass spectra were normalized to the total ion count (TIC). Upon GSK2194069 treatment, the lung cancer cells displayed substantially increased ion intensities of  $m/z$  854.1. Weigt et al. had previously validated this  $m/z$  as malonyl-CoA using MALDI-FT-ICR-based accurate mass determination and tandem-MS experimentation.<sup>[9]</sup> The data indicate intracellular accumulation of malonyl-CoA in response to FASN inhibition (Figure 4B–D).

Due to the high costs of compounds and large reagent volumes (microliters), high-throughput cell screening experiments are usually performed using only a single compound concentration. On the contrary, the droplet microarray platform requires only nanoliters, thereby reducing the overall screening costs. Small volumes also allow more than one drug concentration to be tested in a high-throughput manner, making IC<sub>50</sub> curves a possible outcome of cell-based screening. Multiple repetitions are also more plausible, inevitably leading to a better reproducibility and reliability of the observed results.<sup>[9,25]</sup> The compatibility of DMA slides with MALDI-MSI allows IC<sub>50</sub> curves to be constructed using chemical information obtained by mass-spectrometry. To demonstrate this concept, we analyzed drug responses in A549 cancer cells on the DMA-MSI platform. Adherent-grown cells were incubated for 24 h on 3 mm array spots in the presence of different concentrations of the FASN inhibitor GSK2194069, followed by washing the DMA-ITO slide three times with ice-cold 150-mM ammonium formate at pH 7.4. After air-drying, the slide was spray-coated with DHB matrix. Concentration-response curves of two TIC-normalized peaks ( $[\text{M}+\text{H}]^+$   $m/z$  854.1 and 760.6) were extracted from MALDI-MSI datasets (**Figure 5A,B**). Endogenous malonyl-CoA signal ( $[\text{M}+\text{H}]^+$  854.1  $\pm$  0.2 Da) in A549 cells demonstrated a four-fold change (FC: treated cells/vehicle control) increase, demonstrating the possibility to use MALDI-MSI as a relative quantitative readout for cell-based compound profiling on DMA-ITO slides (Figure 5A). The IC<sub>50</sub> value (marked with an asterisk) derived from this concentration-response curve matches previously described results obtained with a mechanistic MALDI-TOF-MS cell-based assay

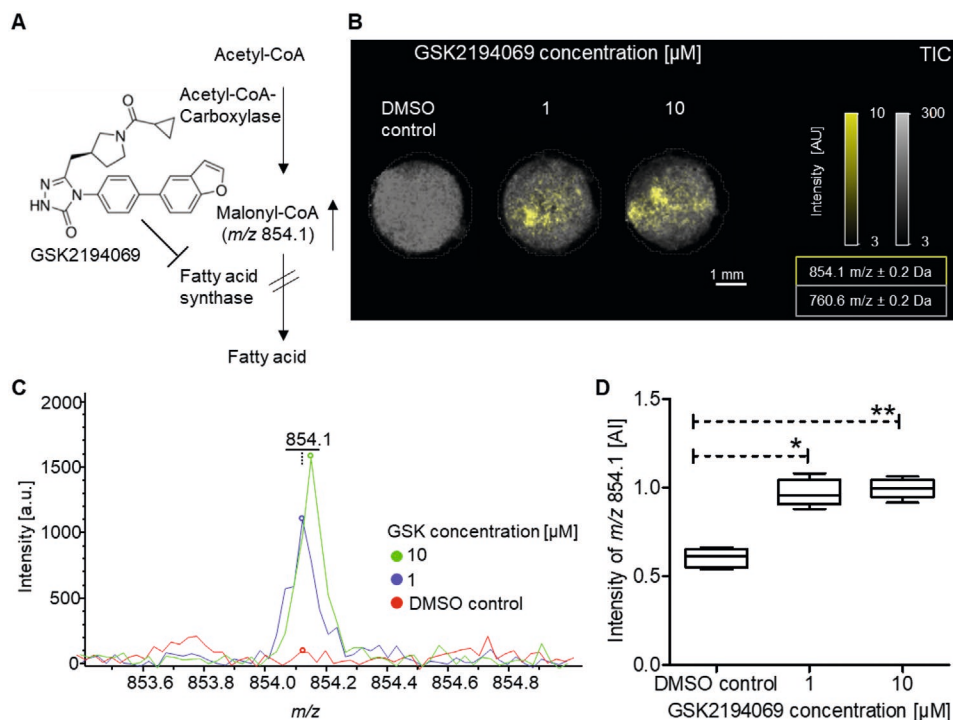


**Figure 4.** Proof of Principle of New DMA-MSI Platform to Analyze Inhibition of FASN Based on MSI of Cellular Malonyl-CoA Accumulation as Response Marker in A549 Cancer Cells. A) Chemical structure of GSK2194069, a selective fatty acid synthase (FASN) inhibitor that leads to intracellular accumulation of the FASN substrate malonyl-Coenzyme (malonyl-CoA). B–D) A549 cells were seeded in assay medium in 3 mm droplet microarrays on indium tin oxide (DMA-ITO) and were treated for 24 h with two high concentrations of GSK2194069 or dimethyl sulfoxide (DMSO) as control (0  $\mu$ M FASN inhibitor). Matrix-assisted laser desorption/ionization-time-of-flight (MALDI-TOF) mass spectra were pre-processed using SCiLS Lab and TIC-normalized ion intensities are shown. B) The spatial distribution of malonyl-CoA ( $m/z$  854.1; yellow) was visualized as ion intensity map using flexImaging software. The spatial signal distribution of the tentative membrane lipid (phosphatidylcholine; PC 34:1) is presented in gray for comparison. C) Original TIC-normalized spectra of  $m/z$  854.1 from randomly chosen single signal-bearing pixels of inhibitor-treated and untreated array positions analyzed in flexAnalysis. D) Malonyl-CoA is significantly increased in GSK2194069-treated cells compared to untreated cells. The mean ion intensity of  $m/z$  854.1 from five technical replicates ( $n = 5$ ) within 3 mm droplet array was plotted against inhibitor concentration and expressed as median  $\pm$  interquartile range (1st and 3rd quartile) by Tukey boxplot with whiskers representing the minimum and maximum values. For the non-normally distributed data one-way Kruskal–Wallis testing followed by Dunn’s Multiple Comparison post-hoc test was carried out across groups (\*  $p \leq 0.05$  and \*\*  $p \leq 0.01$ ).

of FASN inhibition using standard 384-well steel targets.<sup>[15]</sup> When plotted against inhibitor concentration, the normalized intensity fold-change for an endogenous lipid (tentatively assigned phosphatidylcholine: PC (34:1) ( $[M+H]^+$   $m/z$  760.6  $\pm$  0.2 Da)) showed a moderately decreasing concentration-response curve. This may indicate successful inhibition of de novo synthesis of fatty acids and functionally coupled inhibition of phospholipid synthesis (Figure 5B). The corresponding MALDI-MSI ion image (Figure 5C) shows the spatial signal distribution of presumably PC (34:1) in red, and malonyl-CoA in green. The spatial distribution of analytes of interest was visualized as ion intensity maps. The triplicates of the experiment shown in Figure 5C demonstrate both perfect reproducibility of the method, and homogeneity of the spot size and shape owing to the hydrophilic-superhydrophobic borders.

### 3. Conclusions

In this study we have demonstrated hyphenation of two powerful technologies: droplet microarrays (DMA) and MALDI mass spectrometry imaging (MALDI-MSI) to create

a DMA-MSI platform. By combining these technologies, we demonstrate the potential for miniaturized high-throughput cell screening with the biochemical analysis capabilities of mass spectrometry in a single platform. We have established a method for the creation of hydrophilic-superhydrophobic microarrays on conductive ITO slides, showing that confinement of droplets by superhydrophobic borders improves robustness of the matrix application, facilitates spot positioning and increases signal homogeneity and sensitivity of the detection. Using this platform, we have demonstrated highly miniaturized (down to 40 nL and 10 cells per spot) MALDI-TOF-MS cell-based screening assays with label-free quantitative readout using MALDI-MSI. Using concentration-response profiling of the fatty acid synthase inhibitor GSK2194069 in A549 lung cancer cells as an example,  $IC_{50}$  curves were determined based on the chemical composition of the cell surface. The uniqueness of the DMA-MSI platform for cell-based assays lies in the possibility to perform both optical microscopy and mass-spectrometric readouts using the same cell microarray with a minimum number of preparative steps, while at the same time maximizing ion yield by using a conductive substrate.

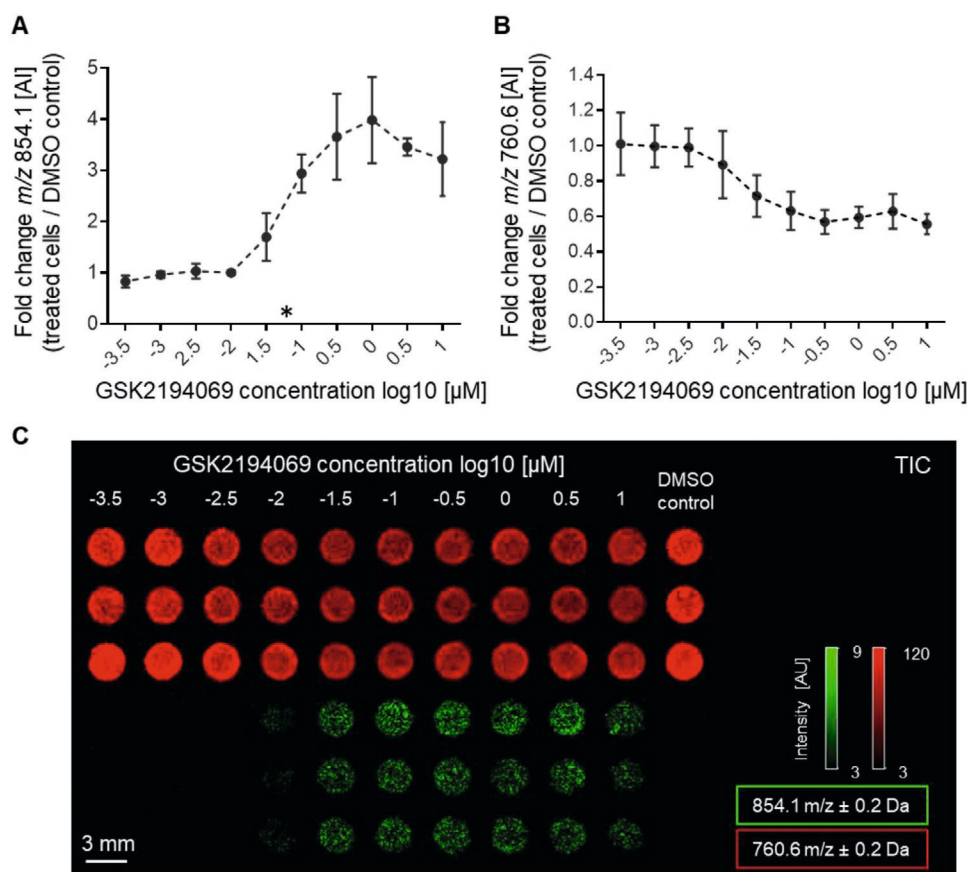


**Figure 5.** Quantitative Analysis of the GSK20194069 Drug Response in A549 Cancer Cells on the DMA-MSI platform. A–C) Concentration-response curve of total ion count (TIC)-normalized extracted features ( $m/z$  854.1 for malonyl-Coenzyme A (malonyl-CoA) and  $m/z$  760.6 tentatively for protonated phosphatidylcholine (PC, 34:1) from the matrix-assisted laser desorption/ionization-mass spectrometry imaging (MALDI MSI) dataset were plotted using GraphPad Prism ( $n = 3$  technical replicates per concentration within 3 mm droplet array). A549 cells were seeded in assay medium onto a droplet microarray-indium tin oxide (DMA-ITO) slide for 18 h and incubated for 24 h with various concentrations of GSK2194069. MALDI-TOF mass spectra were pre-processed using SCiLS Lab and TIC-normalized ion intensities are shown. A) The fold-change (treated cells / dimethyl sulfoxide [DMSO] control,  $n = 3$ ) of endogenous malonyl-CoA ion intensity ( $[M+H]^+ + m/z$  854.1 ± 0.2 Da) in A549 cells was plotted against inhibitor concentration. The IC<sub>50</sub> is marked by an asterisk and derived from this concentration-response curve, matches previously described results.<sup>[9]</sup> Data were presented as mean ± standard deviation (SD) from three technical replicates per concentration within 3 mm droplet array. B) The fold-change (treated cells / DMSO control,  $n = 3$ ) of the tentatively assigned PC (34:1) ( $[M+H]^+ + m/z$  760.6 ± 0.2 Da) was plotted against inhibitor concentration and shows a moderate decrease that may be attributed to inhibition of de novo synthesis of fatty acids. Data were presented as mean ± standard deviation (SD) from three technical replicates per concentration within 3 mm droplet array. C) Corresponding MALDI-MSI ion image (visualized using flexImaging software) shows the spatial signal distribution of PC(34:1) in red and malonyl-CoA in green.

The DMA-MSI platform developed here offers several advantages compared with other technologies:

- Label-free readout while obtaining greater amounts of molecular information for each pixel (namely one mass spectrum per pixel);
- Direct cell culture on DMA-ITO slides, enabling microscopy and MALDI-TOF-MSI on one array;
- Miniaturization of cell assays compared with standard MALDI target plates, resulting in higher spot density (DMA spot size ≤ 0.5 mm);
- Analysis of minute numbers of cells per spot, down to single-cell level;
- A faster overall sample preparation workflow;
- Potential for customization – the porous, cell-supporting coating can be potentially applied to various conductive substrates,<sup>[26]</sup> enabling adaptation of different cell culture formats.<sup>[27]</sup>

Thus, the DMA-MSI platform has great potential for the field of high-throughput cell screening, drug screening, metabolomics, for basic research and drug discovery.

#### 4. Experimental Section

**Materials:** All reagents were of HPLC grade. Milli-Q water (ddH<sub>2</sub>O; Millipore) was prepared in-house. Acetonitrile (ACN), trifluoroacetic acid (TFA) and A549 cells, a human non-small-cell lung cancer cell line, were purchased from Merck (Darmstadt, Germany). Cell culture-grade dimethyl sulfoxide (DMSO), ammonium formate, and penicillin-streptomycin as well as the FASN inhibitor GSK2194069 were obtained from Sigma Aldrich (Munich, Germany). A stock solution of 10 mM malonyl-CoA (Sigma-Aldrich) dissolved in ddH<sub>2</sub>O was stored at -80 °C. RPMI 1640 with stable glutamine (VWR International, Darmstadt, Germany) was used as cell culture medium. Fetal bovine serum (FBS)



and charcoal-stripped FBS for assay medium were from Life Technologies (Darmstadt, Germany). For MALDI-MSI, conductive indium tin oxide (ITO)-coated glass slides were purchased from Bruker Daltonics (Bremen, Germany) and the MALDI matrix 2,5-dihydroxybenzoic acid (DHB) from Alfa Aesar (Karlsruhe, Germany). Porcine brain total lipid extract was purchased from Avanti Polar Lipids (Alabama, USA).

**Preparation of Droplet Microarrays on Conductive Indium tin Oxide (ITO) Slides:** The customized droplet microarray slides (25 mm × 75 mm) were fabricated by Aquarray GmbH (Eggenstein–Leopoldshafen, Germany). The microarray slides were prepared directly on conductive ITO glass slides, and referred to as DMA-ITO slides. Briefly, indium-tin oxide (ITO) glass slides were structured to create nanoporous layer important for increasing both hydrophilicity and hydrophobicity, as well as enhance cell growth, as it was shown that roughness in combination with chemical surface modification tends to enhance cell growth on substrates, especially that of certain primary cells<sup>[28]</sup>. The surface hydroxy groups were silylated to introduce double bonds, which were then functionalized photochemically using either hydrophilic or hydrophobic (fluorinated) thiols to result in highly hydrophilic and superhydrophobic regions, respectively. The coating adhered well and homogeneously onto the ITO surface while being thin enough to avoid insulation of the conductive surface.<sup>[29]</sup> Average ion intensities of various brain total lipid extract lipids on ITO and DMA-ITO were indistinguishable, suggesting comparable conductance of the two coatings. To prove if the conductivity of the ITO glass slide did not change due to additional nanorough layer by spin coating the resistance was always checked with a digital multimeter (Votcraft, Hirschau, Germany) in  $\Omega \text{ cm}^{-2}$  prior cell culturing. Three different formats of DMA-ITO were used: arrays of 5 × 16 spots with side length of 3 mm; 14 × 48 spots with side length of 1 mm and 28 × 84 spots with side length of 0.5 mm.

**Cell Culture on DMA-ITO Slides:** A549 cells were pre-cultured in T75 flasks with RPMI-1640 supplemented with glutamine, 10% (v/v) FBS and 1% (v/v) penicillin/streptomycin at 37 °C at 5% CO<sub>2</sub>. 10% v/v fetal bovine serum (FBS) and 1% v/v penicillin/streptomycin (P/S) at 37 °C with 5% CO<sub>2</sub> atmosphere. For the analysis of miniaturized cell-based assays, A549 cells were seeded at various densities ranging from 707 to 14 cells/mm<sup>2</sup> on three different DMA-ITO slides with array spot sizes of 3, 1, and 0.5 mm. The total cell number per array spot was adjusted as listed in Table 1 in order to keep cell density (cells/mm<sup>2</sup>) comparable. The following culture volumes were used: 5  $\mu\text{L}$ , 150 nL, and 40 nL for DMA-ITO with spot sizes of 3, 1, and 0.5 mm, respectively. Cells were seeded onto DMA-ITO slides using low volume dispenser I-DOT (Dispendix GmbH, Stuttgart, Germany). Afterwards slides were incubated overnight at 37 °C at 5% CO<sub>2</sub>. Subsequently, slides were washed three times with cold 150 mM ammonium formate at pH 7.4. Until MALDI MSI analysis, slides were frozen on dry-ice and stored at –80 °C.

**FASN Inhibition Cell Assay on DMA-MSI Platform:** One day prior to inhibitor treatment, cells were resuspended in concentration  $6.3 \times 10^5 \text{ cells mL}^{-1}$  cell culture medium supplemented with 10% v/v charcoal stripped FBS (assay medium). 8  $\mu\text{L}$  of the cell suspension was seeded per spot on the DMA-ITO slides with 3 mm spot sizes and incubated overnight for 18 h at 37 °C at 5% CO<sub>2</sub>. On the following day, cells were treated for 24 h with GSK2194069. To keep the final DMSO concentration of 0.33% (vol.%) in the assay constant, a ten-step dilution series of 10 mM GSK2194069 in DMSO stock solution was performed in DMSO at ratio of 1: 3.3, obtaining the following concentrations: 3.2, 1.0, 0.3, 0.1, 0.03, 0.01 mM, 3.2, 1.0, 0.3, and 0.1  $\mu\text{M}$ . Each of these concentrations was subsequently diluted with assay medium at a ratio of 1:150 (one volume diluted 150-fold in assay medium), obtaining the following concentrations: 21.1, 6.7, 2.1, 0.67, 0.21, 0.067, 0.021, 0.0067, 0.0021  $\mu\text{M}$ , 0.67 nM. Finally, for all concentrations of FASN inhibitor, one volume of inhibitor (8  $\mu\text{L}$ ) was added to one volume (8  $\mu\text{L}$ ) of cell culture droplets. Final inhibitor concentrations were 10.5, 3.3, 1.1, 0.33, 0.11, 0.033, 0.011  $\mu\text{M}$ , 3.3, 1.1, 0.33 nM and 0.33% DMSO as a vehicle control in a total volume of 16  $\mu\text{L}$  on 3 mm Droplet array (DMA-ITO). After 24 h, slides were washed three times with ice-cold 150 mM ammonium formate at pH 7.4 and were subsequently air-dried.

**Cell Viability Assay:** Live/dead staining of cells cultured on DMA-ITO slides was performed by dispensing 2.5  $\mu\text{L}$ , 50 nL, and 14 nL of solution containing 1.5  $\mu\text{g mL}^{-1}$  Calcein AM (Thermo Scientific) and 1.5  $\mu\text{g mL}^{-1}$  propidium iodide (PI) (Invitrogen, Merelbeke, Belgium) in Dulbecco's PBS to the droplets on 3, 1, and 0.5 mm spots, respectively, using low volume dispenser I-DOT (Dispendix GmbH, Stuttgart, Germany). Cells were incubated for 15 min in cell culture incubator and then imaged using Keyence BZ-9000 microscope (KEYENCE, Osaka, Japan). The number of Calcein-positive (live) and PI-positive (dead) cells was estimated using ImageJ software, and viability of cells was calculated as a ratio of number of live cells to total number of cells (sum of live cells and dead cells).

**MALDI-TOF Mass Spectrometry Imaging:** For MALDI MSI, washed DMA-ITO cell arrays were air-dried or vacuum-dried after freezing for 15 min at RT. DHB matrix was prepared at a concentration of 60 mg mL<sup>-1</sup> in ACN/ddH<sub>2</sub>O/TFA (50/49.9/0.1; v/v/v) unless indicated otherwise. Matrix deposition on cells grown on DMA-ITO slides was performed by spray-coating using a HTX TM 5-sprayer (HTX Technologies, LLC, Chapel Hill, NC, USA): Briefly, five layers were sprayed at 100  $\mu\text{L min}^{-1}$  matrix flow rate and 1200 mm min<sup>-1</sup> spray-head velocity with 3 mm distance between sprayed lines (CC pattern). Spray nozzle height was set to 40 mm from the ITO slide and temperature was heated to 75 °C with a pressure of 10 psi and 2 L min<sup>-1</sup> of gas flow rate. MALDI-MSI experiments were performed using a rapiflex MALDI-TOF mass spectrometer (Bruker Daltonics, Bremen, Germany) equipped with a 10 kHz smartbeam 3D laser. Data was acquired in reflector positive ion mode within an  $m/z$  range of 500–1200 using a raster width of 50  $\mu\text{m}$  for the 3 mm DMA or 25  $\mu\text{m}$  for the 1- and 0.5 mm DMA employing fmsControl 4.1.8 and flexImaging 5.0.89.0 softwares (Bruker Daltonics). Focus and laser power settings were optimized with a sampling rate of 1.25 for 50 or 25  $\mu\text{m}$  pixel size with 200 shots per pixel. FASN inhibition analysis was executed at a lateral step-size of 100  $\mu\text{m}$  over a mass range of  $m/z$  400–1000 summing up 250 laser shots per pixel with a sampling rate of 1.25. External quadratic calibration of the rapiflex was typically performed using porcine brain total lipid extract, but a mixture of the lysophosphatidylcholine LPC(18:1) ( $[M+H]^+$  522.355), the phosphatidylcholine, PC(34:1) ( $[M+H]^+$  760.585 and  $[M+K]^+$  798.541) and malonyl-CoA ( $[M+H]^+$  854.123) for the FASN inhibition assay.

**Pre-Processing and Visualization of MALDI MS Imaging Data:** The pre-processing of MALDI imaging data was executed using the SCiLS Lab 2019 software (Bruker Daltonics). Thus, baseline subtraction was performed using the top-hat algorithm and all mass spectra were divided by their Total Ion Count (TIC), so that all spectra in a dataset have the same integrated area under the spectrum. The spatial distribution of a selected mass to charge ratio ( $m/z$ ) of an ionized molecule was visualized as TIC-normalized ion intensity map using SCiLS Lab 2019 or flexImaging software version 5.0 from Bruker Daltonics.

For data comparison in Figure 2D, TIC-normalized mean spectra of regions-of-interest (ROI) drawn in SCiLS Lab were exported into mMass (V5.5.0)<sup>[30]</sup> in order to flip spectra vertically to detect any differences between those two mass spectra (“butterfly plot”). For an automated and unsupervised segmentation analysis in Figure 3B, all TIC-normalized mass spectra were analyzed in SCiLS Lab using  $m/z$  value  $760.6 \pm 0.1 \text{ Da}$  by bisecting k-means algorithm and the correlation distance metric without denoising. In Figures 3E and 4C, original TIC-normalized spectra of specific  $m/z$ -values from randomly chosen single signal-bearing pixels were extracted and analyzed with flexAnalysis 3.4 software (Bruker Daltonics) or mMass. Peak quality parameters were signal to noise threshold ( $S/N$ ) = 6 and peak width = 0.1 Da at 75% peak height. Original mass spectra were externally re-calibrated in flexAnalysis or in mMass. In Figure 5A,B, concentration-response curves from the FASN inhibition assay were plotted with GraphPad Prism software version 5.0 (GraphPad). Therefore, the mean ion intensity of TIC-normalized spectra from  $m/z$ -values 854.1 and 760.6  $\pm 0.2 \text{ Da}$  were extracted from ROIs drawn in SCiLS Lab around the 3 mm droplet spots and exported into GraphPad Prism. For each of these  $m/z$  values relative quantification was performed by determining the fold-change (FC) of ion intensity from inhibitor-treated samples versus the vehicle DMSO control. The fold change was plotted against inhibitor concentration.

Data were presented as mean  $\pm$  standard deviation (SD) from three technical replicates per concentration within 3 mm droplet array.

**Statistical Analysis:** In order to demonstrate utility of the DMA-MSI platform for a FASN inhibitor assay, the MALDI imaging data was pre-processed in SCiLS Lab as described above. For Figure 4D the intensity of the Malonyl-CoA ion signal ( $m/z$  854.1  $\pm$  0.2 Da) was extracted from the TIC-normalized average spectra from ROIs drawn in SCiLS Lab around the 3 mm droplet spots. Extracted signals for all tested inhibitor concentrations and vehicle control were imported into GraphPad Prism for statistical analysis. Therefore, the mean ion intensity of  $m/z$  854.1 from five technical replicates was plotted against inhibitor concentration as median  $\pm$  interquartile range by Tukey boxplot. For the non-normally distributed data one-way Kruskal-Wallis test was carried out across groups. Pairwise comparisons of ion intensity from inhibitor-treated samples versus the vehicle DMSO control were performed using Dunn's Multiple Comparison post-hoc test and significant differences were reported as \*  $p \leq 0.05$  and \*\*  $p \leq 0.01$ .

Data presentation and sample size ( $n$ ) for each analysis was indicated in the corresponding figure legend.

## Supporting Information

Supporting Information is available from the Wiley Online Library or from the author.

## Acknowledgements

C.H. and P.A.L. contributed equally to this work. This study was supported by the Ministry of Science and Art (MWK) Baden-Württemberg MALDIDROPScreen (7533-7-11.10-12). C.H. is grateful for funding of a rapiflex MALDI-TOF mass spectrometer by the Hector Foundation II. This work was funded by the German Federal Ministry of Research (BMBF) as part of the Innovation Partnership M<sup>2</sup>Aind, project SM<sup>2</sup>all (03FH81011A) within the framework FH-Impuls (to CH).

Open access funding enabled and organized by Projekt DEAL.

## Conflict of Interest

The authors declare no conflict of interest.

## Data Availability Statement

Raw experimental data are available upon request.

## Keywords

droplet microarray, drug discovery, fatty acid synthase, MALDI imaging, MALDI mass spectrometry, miniaturized cell-based assay

Received: September 14, 2020

Revised: December 23, 2020

Published online:

- [1] W. F. An, N. Tolliday, *Mol. Biotechnol.* **2010**, *45*, 180.  
 [2] a) D. C. Swinney, J. Anthony, *Nat. Rev. Drug Discovery* **2011**, *10*, 507;  
 b) D. T. Chiu, O. Orwar, *Drug Discov. World* **2004**, *Spring* **2004**, *5*, 45;  
 c) W. E. Childers, K. M. Elokely, M. Abou-Gharbia, *ACS Med. Chem. Lett.* **2020**, *11*, 1820.

- [3] a) B. B. Aggarwal, G. Sethi, V. Baladandayuthapani, S. Krishnan, S. Shishodia, *J. Cell. Biochem.* **2007**, *102*, 580; b) A. Luengo, D. Y. Gui, M. G. Vander Heiden, *Cell Chem. Biol.* **2017**, *24*, 1161; c) A. Heguy, A. A. Stewart, J. D. Haley, D. E. Smith, J. G. Foulkes, *Gene Expr.* **1995**, *4*, 337; d) L. Zhao, P. Liu, G. Boncompain, F. Loos, S. Lachkar, L. Bezu, G. Chen, H. Zhou, F. Perez, O. Kepp, G. Kroemer, *Sci. Rep.* **2018**, *8*, 14966; e) S. Senese, Y. C. Lo, D. Huang, T. A. Zangle, A. A. Gholkar, L. Robert, B. Homet, A. Ribas, M. K. Summers, M. A. Teittel, R. Damoiseaux, J. Z. Torres, *Cell Death Dis.* **2014**, *5*, e1462.  
 [4] a) M. Boutros, F. Heigwer, C. Laufer, *Cell* **2015**, *163*, 1314; b) T. L. Riss, R. A. Moravec, A. L. Niles, S. Duellman, H. A. Benink, T. J. Worzella, et al. in *Assay Guidance Manual* (Eds: S. Markossian, G. S. Sittampalam, A. Grossman, K. Brimacombe, M. Arkin, D. Auld, et al.), Bethesda, MD **2004**; c) I. Becher, A. Dittmann, M. M. Savitski, C. Hopf, G. Drewes, M. Bantscheff, *ACS Chem. Biol.* **2014**, *9*, 1736.  
 [5] a) I. Miller, M. Min, C. Yang, C. Tian, S. Gookin, D. Carter, S. L. Spencer, *Cell Rep.* **2018**, *24*, 1105; b) C. Lema, A. Varela-Ramirez, R. J. Aguilera, *Curr. Cell Biochem.* **2011**, *1*, 1.  
 [6] X. He, S. Memczak, J. Qu, J. C. I. Belmonte, G.-H. Liu, *Nat. Metabol.* **2020**, *2*, 293.  
 [7] B. Munteanu, B. Meyer, C. von Reitzenstein, E. Burgermeister, S. Bog, A. Pahl, M. P. Ebert, C. Hopf, *Anal. Chem.* **2014**, *86*, 4642.  
 [8] a) S. Schulz, M. Becker, M. R. Groseclose, S. Schadt, C. Hopf, *Curr. Opin. Biotechnol.* **2019**, *55*, 51; b) P. Arranz-Gibert, B. Guixar, R. Prades, S. Ciudad, E. Giralt, M. Teixidó, *Sci. Rep.* **2019**, *9*, 4875; c) D. Abu Sammour, C. Marsching, A. Geisel, K. Erich, S. Schulz, C. Ramallo Guevara, J.-H. Rabe, A. Marx, P. Findeisen, P. Hohenberger, C. Hopf, *Sci. Rep.* **2019**, *9*, 10698; d) K. Erich, D. A. Sammour, A. Marx, C. Hopf, *Biochim. Biophys. Acta, Proteins Proteomics* **2017**, *1865*, 907; e) I. Hinsenkamp, S. Schulz, M. Roscher, A.-M. Suhr, B. Meyer, B. Munteanu, J. Fuchser, S. O. Schoenberg, M. P. A. Ebert, B. Wängler, C. Hopf, E. Burgermeister, *Neoplasia* **2016**, *18*, 500.  
 [9] D. Weigt, C. A. Parrish, J. A. Krueger, C. A. Oleykowski, A. R. Rendina, C. Hopf, *Cell Chem. Biol.* **2019**, *26*, 1322.  
 [10] D. Weigt, D. A. Sammour, T. Ulrich, B. Munteanu, C. Hopf, *Sci. Rep.* **2018**, *8*, 11260.  
 [11] R. E. Heap, A. Segarra-Fas, A. P. Blain, G. M. Findlay, M. Trost, *Analyst* **2019**, *144*, 6371.  
 [12] M. S. Unger, L. Schumacher, T. Enzlein, D. Weigt, M. J. Zamek-Gliszczynski, M. Schwab, A. T. Nies, G. Drewes, S. Schulz, F. B. M. Reinhard, C. Hopf, *Anal. Chem.* **2020**, *92*, 11851.  
 [13] K. Beeman, J. Baumgärtner, M. Laubenheimer, K. Hergesell, M. Hoffmann, U. Pehl, F. Fischer, J. C. Pieck, *SLAS Discovery* **2017**, *22*, 1203.  
 [14] R. P. Simon, M. Winter, C. Kleiner, R. Ries, G. Schnapp, A. Heimann, J. Li, L. Zuvella-Jelaska, T. Bretschneider, A. H. Luippold, W. Reindl, D. Bischoff, F. H. Büttner, *SLAS Discovery* **2020**, *25*, 372.  
 [15] M. Winter, R. Ries, C. Kleiner, D. Bischoff, A. H. Luippold, T. Bretschneider, F. H. Büttner, *SLAS Technol.* **2018**, *24*, 209.  
 [16] a) A. J. Ibáñez, S. R. Fagerer, A. M. Schmidt, P. L. Urban, K. Jefimovs, P. Geiger, R. Dechant, M. Heinemann, R. Zenobi, *Proc. Natl. Acad. Sci. U. S. A.* **2013**, *110*, 8790; b) J. Krismer, J. Sobek, R. F. Steinhoff, R. Brönnimann, M. Pabst, R. Zenobi, *Methods Mol. Biol.* **2020**, *2064*, 113.  
 [17] K. Scupakova, F. Dewez, A. K. Walch, R. M. A. Heeren, B. Balluff, *Angew. Chem. Int. Ed.* **2020**, *59*, 17447.  
 [18] a) K. D. Duncan, J. Fyrestam, I. Lanekoff, *Analyst* **2019**, *144*, 782; b) C. L. Correa-Martínez, E. A. Idelevich, K. Sparbier, T. Kuczus, M. Kostrzewa, K. Becker, *Sci. Rep.* **2020**, *10*, 4988.  
 [19] J. Koubek, O. Uhlik, K. Jecna, P. Junkova, J. Vrkoslavova, J. Lipov, V. Kurzawova, T. Macek, M. Mackova, *Int. Biodeterior. Biodegrad.* **2012**, *69*, 82.

- [20] a) K. Mallah, J. Quanico, A. Raffo-Romero, T. Cardon, S. Aboulouard, D. Devos, F. Kobeissy, K. Zibara, M. Salzet, I. Fournier, *Anal. Chem.* **2019**, *91*, 11879; b) M. Benazouz, B. Hakim, J. L. Debrun, *Rapid Commun. Mass Spectrom.* **1998**, *12*, 1018.
- [21] a) G. P. Zeegers, B. F. Günthardt, R. Zenobi, *J. Am. Soc. Mass Spectrom.* **2016**, *27*, 699; b) A. A. Popova, K. Demir, T. G. Hartanto, E. Schmitt, P. A. Levkin, *RSC Adv.* **2016**, *6*, 38263.
- [22] a) A. A. Popova, C. Depew, K. M. Permana, A. Trubitsyn, R. Peravali, J. Á. G. Ordiano, M. Reischl, P. A. Levkin, *SLAS Technol.* **2016**, *22*, 163; b) A. A. Popova, S. M. Schillo, K. Demir, E. Ueda, A. Nesterov-Mueller, P. A. Levkin, *Adv. Mater.* **2015**, *27*, 5217.
- [23] A. A. Popova, K. Demir, T. G. Hartanto, E. Schmitt, P. A. Levkin, *RSC Adv.* **2016**, *6*, 38263.
- [24] a) A. A. Popova, T. Tronser, K. Demir, P. Haitz, K. Kuodyte, V. Starkuviene, P. Wajda, P. A. Levkin, *Small* **2019**, *15*, 1901299; b) C. Haslam, J. Hellicar, A. Dunn, A. Fuetterer, N. Hardy, P. Marshall, R. Paape, M. Pemberton, A. Resemannand, M. Leveridge, *J. Biomol. Screen* **2016**, *21*, 176; c) J. Chandler, C. Haslam, N. Hardy, M. Leveridge, P. Marshall, *SLAS Discovery* **2016**, *22*, 1262.
- [25] a) S. J. Chanock, T. Manolio, M. Boehnke, E. Boerwinkle, D. J. Hunter, G. Thomas, J. N. Hirschhorn, G. Abecasis, D. Altshuler, J. E. Bailey-Wilson, L. D. Brooks, L. R. Cardon, M. Daly, P. Donnelly, J. F. Fraumeni, Jr., N. B. Freimer, D. S. Gerhard, C. Gunter, A. E. Guttmacher, M. S. Guyer, E. L. Harris, J. Hoh, R. Hoover, C. A. Kong, K. R. Merikangas, C. C. Morton, L. J. Palmer, E. G. Phimister, J. P. Rice, J. Roberts, C. Rotimi, M. A. Tucker, K. J. Vogan, S. Wacholder, E. M. Wijsman, D. M. Winn, F. S. Collins, *Nature* **2007**, *447*, 655; b) C. J. Lord, N. Quinn, C. J. Ryan, *bioRxiv* **2020**, 646810.
- [26] a) S. J. Lord, K. B. Velle, R. D. Mullins, L. K. Fritz-Laylin, *J. Cell Biol.* **2020**, *219*, e202001064; b) C. Q. Peng, Y. S. Thio, R. A. Gerhardt, *Nanotechnology* **2008**, *19*, 505603.
- [27] a) Y. Leterrier, L. Médico, F. Demarco, J. A. E. Månson, U. Betz, M. F. Escolà, M. Kharrazi Olsson, F. Atamny, *Thin Solid Films* **2004**, *460*, 156; b) T. Agarwal, P. Biswas, S. Pal, T. K. Maiti, S. Chakraborty, S. K. Ghosh, R. Dhar, *ACS Appl. Bio Mater.* **2020**, *3*, 2522; c) F. Tobias, J. C. McIntosh, G. J. LaBonia, M. W. Boyce, M. R. Lockett, A. B. Hummon, *Anal. Chem.* **2019**, *91*, 15370; d) J. Li, E. H. Hill, L. Lin, Y. Zheng, *ACS Nano* **2019**, *13*, 3783; e) M. Kopeć, S. Tas, M. Cirelli, R. van der Pol, I. de Vries, G. J. Vancso, S. de Beer, *ACS Appl. Polym. Mater.* **2019**, *1*, 136; f) J. Rull-Barrull, M. d'Halluin, E. Le Grogneq, F. X. Felpin, *J. Mater. Chem. C* **2017**, *5*, 5154.
- [28] a) F. Gentile, L. Tirinato, E. Battista, F. Causa, C. Liberale, E. M. di Fabrizio, P. Decuzzi, *Biomaterials* **2010**, *31*, 7205; b) M. Mirbagheri, V. Adibnia, B. R. Hughes, S. D. Waldman, X. Banquy, D. K. Hwang, *Mater. Horiz.* **2019**, *6*, 45; c) H. Shindo, M. Kuwamori, M. Taniguchi, *J. Biosci. Bioeng.* **2012**, *113*, 661.
- [29] a) M. Z. H. Khan, *Cogent Eng.* **2016**, *3*, 1170097; b) P. K. H. Ho, M. Granström, R. H. Friend, N. C. Greenham, *Adv. Mater.* **1998**, *10*, 769.
- [30] M. Strohal, D. Kavan, P. Novák, M. Volný, V. Havlíček, *Anal. Chem.* **2010**, *82*, 4648.